

Global optimization of 8-10 atom palladium-iridium nanoalloys at the DFT level

Davis, Jack; Horswell, S.L.; Johnston, R.L.

DOI:

[10.1021/jp408519z](https://doi.org/10.1021/jp408519z)

License:

None: All rights reserved

Document Version

Peer reviewed version

Citation for published version (Harvard):

Davis, J, Horswell, SL & Johnston, RL 2014, 'Global optimization of 8-10 atom palladium-iridium nanoalloys at the DFT level', *The Journal of Physical Chemistry A*, vol. 118, no. 1, pp. 208-214.
<https://doi.org/10.1021/jp408519z>

[Link to publication on Research at Birmingham portal](#)

Publisher Rights Statement:

Final Version of Record published as above
Validated 9/8/2016

General rights

Unless a licence is specified above, all rights (including copyright and moral rights) in this document are retained by the authors and/or the copyright holders. The express permission of the copyright holder must be obtained for any use of this material other than for purposes permitted by law.

- Users may freely distribute the URL that is used to identify this publication.
- Users may download and/or print one copy of the publication from the University of Birmingham research portal for the purpose of private study or non-commercial research.
- User may use extracts from the document in line with the concept of 'fair dealing' under the Copyright, Designs and Patents Act 1988 (?)
- Users may not further distribute the material nor use it for the purposes of commercial gain.

Where a licence is displayed above, please note the terms and conditions of the licence govern your use of this document.

When citing, please reference the published version.

Take down policy

While the University of Birmingham exercises care and attention in making items available there are rare occasions when an item has been uploaded in error or has been deemed to be commercially or otherwise sensitive.

If you believe that this is the case for this document, please contact UBIRA@lists.bham.ac.uk providing details and we will remove access to the work immediately and investigate.

Global optimisation of 8–10 atom palladium-iridium nanoalloys at the DFT level

Jack B. A. Davis, Sarah L. Horswell, and Roy L. Johnston*

School of Chemistry, University of Birmingham, Edgbaston, B15 2TT, Birmingham, United Kingdom

E-mail: r.l.johnston@bham.ac.uk

Abstract

The global optimisation of $N=8-10$ $\text{Pd}_n\text{Ir}_{N-n}$ clusters has been carried out using the Birmingham Cluster Genetic Algorithm (BCGA). Structures are evaluated directly using density functional theory (DFT), which has allowed the identification of Ir and Ir-rich PdIr cubic global minima, displaying a strong tendency to segregate. The ability of the searches to find the global minimum has been assessed using a homotop search method, which shows a high degree of success. The role of spin in the system has been considered through a series of spin-restricted re-optimisations of BCGA-DFT minima. The preferred spin of the clusters is found to vary widely with composition, showing no overall trend in lowest energy multiplicities.

Introduction

It is well established that alloying can increase the activity and/or the selectivity of metal catalysts.¹ On the nanoscale, nanoalloys have the potential to combine this alloying effect with tunable properties for use in specific processes.^{2,3} The structural characterisation of nanoalloys is a vital

*To whom correspondence should be addressed

step toward understanding their role in catalysis. Several methods exist, including basin-hopping and genetic algorithms.³⁻⁵

Noble metals are being widely investigated for use in catalysis. Small iridium clusters show promise in both heterogeneous and homogeneous catalysis, including activity in the ring opening catalysis of naphthenes.⁶ Palladium-iridium nanoalloy catalysts show activity in tetralin interconversion, the hydrogenation of benzonitrile and in the preferential oxidation of CO for the elimination of impurities in H₂ production.⁷⁻⁹

Previous density functional theory (DFT) studies of small Ir clusters, using ultrasoft pseudopotentials and PBE exchange-correlation functionals, have predicted a simple cubic arrangement for clusters of up to 48-atoms, before there is a transition to the FCC structure found in the bulk. This is coupled with results from CCSD calculations which also predict a cubic structure.¹⁰⁻¹² DFT studies of small Pd clusters have also been conducted.²⁰ These, however, were not exhaustive searches of the conformational space.

In this study the global optimisation of $N=8-10$ Pd_{*n*}Ir _{$(N-n)$} clusters is performed, where N is the total number of atoms and n the number of Pd atoms. Global optimisation is carried out using the Birmingham Cluster Genetic Algorithm (BCGA) which allows global optimisation directly at the DFT level, utilising an interface to the plane-wave DFT PWscf code, within Quantum Espresso.¹³ This provides an unbiased search starting from entirely random coordinates and enables the identification of size specific effects not usually described by empirical methods, such as the Gupta potential.^{14,15}

As a result of the 5d⁷6s² ground state electronic configuration of Ir, and low lying states originating from its 5d⁸6s¹ configuration, the spin of any Ir _{N} and Pd_{*n*}Ir _{$(N-n)$} clusters must be considered.¹⁶ The role of spin has not been widely investigated for Ir clusters but has been shown to play a role.¹² The spin of the pure and alloyed clusters is investigated through the use of spin-restricted calculations on BCGA-DFT global minima using atomic-orbital based DFT calculations in the NWChem package.¹⁷ Spin-unrestricted QE calculations are not carried out within the BCGA due to the high computational cost of converging both the spin and geometry of the system.

Methodology

In the present study the BCGA, using an interface to the PWscf DFT code within the Quantum Espresso (QE) package, has been adopted for the global optimisation of Pd-Ir nanoalloy structures. The BCGA is a genetic algorithm for the structural characterisation of nanoparticles and nanoalloys. The interface to QE allows the energy landscape of a system to be explored at the DFT level.^{5,13,15}

The initial population consists of a number of randomly generated cluster geometries, $N_{pop} = 10 - 40$. The BCGA is a “Lamarckian” type GA with fitness being assigned to locally minimised structures at each step of the GA according to their energy. Structures with the lowest energies have the highest fitness, V_{clus} . Here the energy of each member of the population will be calculated using a PWscf calculation.

Competition between clusters is simulated by roulette wheel selection followed by crossover.⁵ Crossover occurs according to the Deaven and Ho cut and splice method and continues until a predetermined number of offspring, N_{off} , have been generated.¹⁸ Mutation is carried out to ensure population diversity is maintained. All members of the population have a probability, p_{mut} , of being selected for mutation. The BCGA contains a number of mutation schemes, including, *atom displacement*, *twisting*, *cluster replacement* and *atom permutation*.

This process of selection, crossover and mutation is repeated for a number of *generations*. The population is considered converged when the range of energies goes unchanged for a number of generations.⁵

QE calculations were carried out using PAW pseudopotentials, taking scalar relativistic effects into account. The Perdew-Burke-Ernzerhof (PBE) exchange correlation functional is used within the generalised gradient approximation (GGA). An energy cut-off (E_{cut}) of 55 Ry is used with the default density cutoff, to ensure fast SCF steps and quick convergence. The Fermi-Dirac smearing scheme was employed with a smearing width of 0.02 to improve metallic convergence.

Spin-polarised reminimisations of the BCGA-DFT global minima were carried out with the orbital-based DFT package NWChem.¹⁷ Def2-TZVP basis sets and PBE exchange correlation

functionals were employed.¹⁹ Geometry optimisations were carried out using the DRIVER module.

Excess energies (Δ) are calculated to determine the stability of bimetallic clusters relative to the monometallic species, or the energy associated with alloying. Δ is defined as

$$\Delta = E(A_m B_n) - m \frac{E(A_N)}{N} - n \frac{E(B_N)}{N}, \quad (1)$$

DFT binding energies (E_b) are computed from

$$E_b = \frac{1}{N} [E_{(A_m B_n)} - mE_A - nE_B], \quad (2)$$

where $E_{A_m B_n}$ is the total energy of the cluster and $E_{A/B}$ are the energies of the single atoms.

Results and discussion

The proposed global minima for $N=8-10$ $\text{Pd}_n\text{Ir}_{(N-n)}$ clusters found using the BCGA-DFT approach are shown in figures 1-3. Tables listing the structures and point groups of all clusters are given in the supporting information.

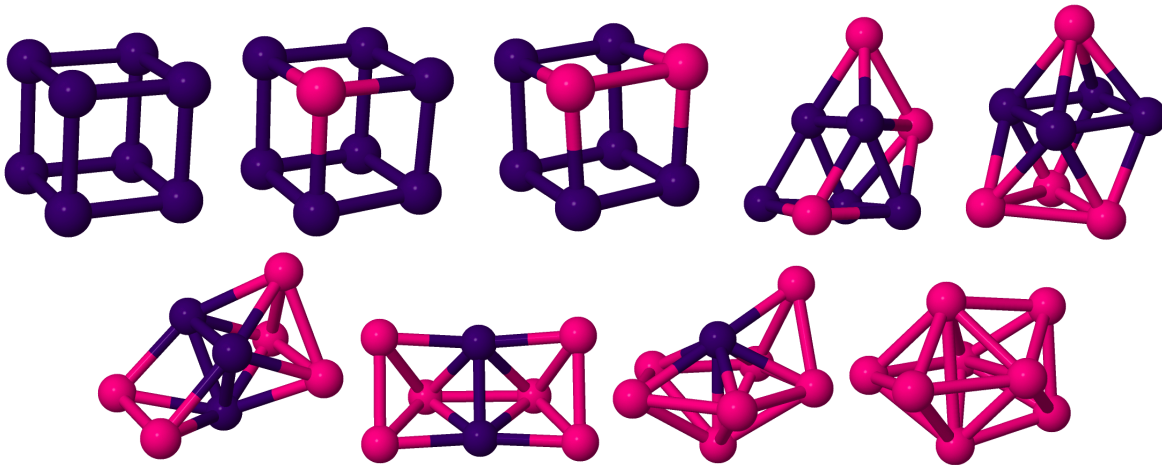


Figure 1: Global minima for 8-atom $\text{Pd}_n\text{Ir}_{(8-n)}$ clusters. Pd and Ir are shown in pink and purple, respectively.

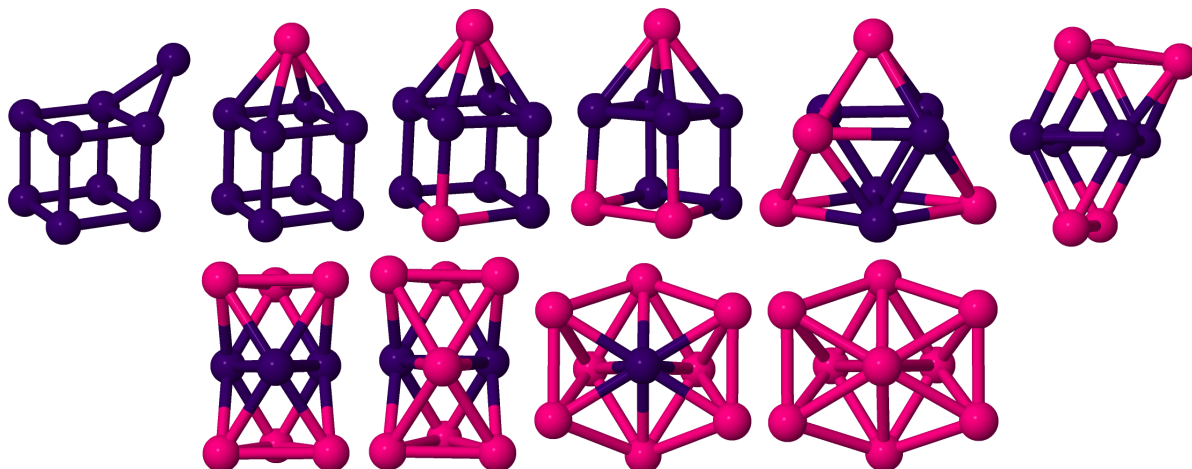


Figure 2: Global minima for 9-atom $\text{Pd}_n\text{Ir}_{(9-n)}$ clusters.

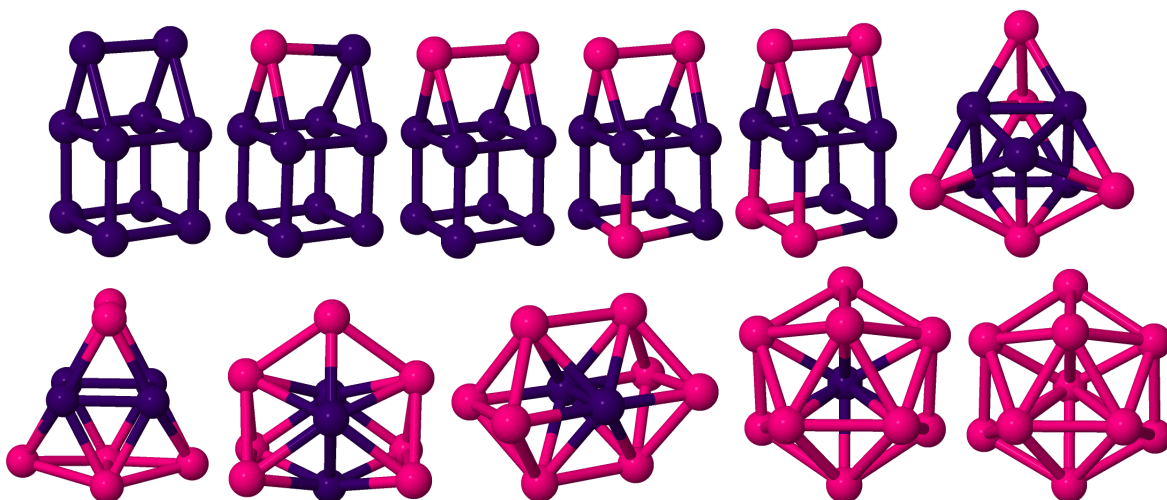


Figure 3: Global minima for 10-atom $\text{Pd}_n\text{Ir}_{(10-n)}$ clusters.

The Ir_8 global minimum (GM) is a cube, as previously reported.^{10–12} When doped with up to two Pd-atoms the cube remains the GM. When three Pd-atoms are added the structure changes to a C_s structure based on a capped trigonal prism with a four atom square Ir fragment. The Pd_8 GM is a D_{2d} dodecahedral structure, as previously reported.²⁰ Upon successive iridium doping, the structure changes to a C_s capped pentagonal bipyramid and then to a C_{2h} structure formed from two edge-sharing square pyramids.

The Ir_9 GM is an edge-bridged cube, also as previously reported.¹¹ As Pd is doped into the

structure, the cap switches from an edge to a face with Pd occupying the capping site. This is the case for PdIr₈, Pd₂Ir₇ and Pd₃Ir₆. The first Pd dopant caps a face, with the second and third forming a Pd-Pd bond on the face opposite to the cap. Pd₄Ir₅ and Pd₅Ir₄ both retain square Ir fragments. Pd₉ is an C_{2v} icosahedral structure, again as previously reported.²⁰ Pd₈Ir₁ retains this structure, with the iridium dopant occupying the central site. Pd₇Ir₂ and Pd₆Ir₃ are both structures of two face-sharing octahedra, with Pd₆Ir₃ having a central Ir₃ triangle and D_{3h} symmetry.

The Ir₁₀ GM is a cube with a two-atom bridge over a face, forming a house-like structure, differing from the two-atom bridged edge structure reported by Wang et al., shown in figure 4.¹¹ When minimised with PWscf the BCGA-GM is found to be more favourable by 0.34 eV. This 'house' structure remains the GM for PdIr₉, Pd₂Ir₈, Pd₃Ir₇ and Pd₄Ir₆. Pd is found to occupy preferentially the face-bridging sites, forming a Pd-Pd bond for Pd₂Ir₈. The third and fourth Pd atoms form a bond on the opposite face.

The GM for Pd₁₀ and Pd₉Ir are found to be a C_{3v} structure corresponding to an incomplete centred-icosahedron. In Pd₉Ir, the Ir atom occupies the exposed icosahedral core site. This differs from the edge-sharing octahedra previously reported for Pd₁₀ by Ahlrichs et al., shown in figure 5.²⁰ When minimised with PWscf, the BCGA-GM is found to be more favourable by 0.2 eV. The D_{2h} edge-sharing structure is, however, found as the GM for Pd₈Ir₂.

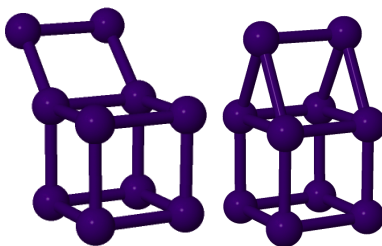


Figure 4: Lowest energy structure reported by Wang et al., left, and the lower energy GM from the BCGA-DFT, right, for Ir₁₀.

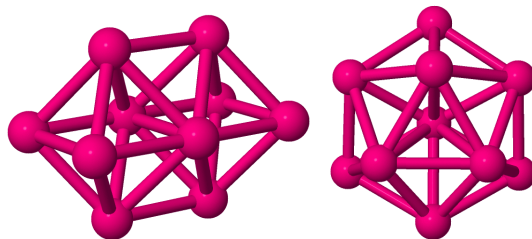


Figure 5: Lowest energy structure reported by Ahlrichs et al., left, and the lower energy GM from the BCGA-DFT, right, for Pd₁₀.

The relative strengths of homo- and heteronuclear bonding can be used to predict the extent of mixing in a system. The binding energies of the pure and heterometallic dimers are listed in table 1. The triplet and quintet states for Pd₂ and Ir₂ agree with previous work.^{11,20} The binding energy of Pd₂ is slightly higher than that published by Ahlrichs et al of 0.663 eV.²⁰ The value of 2.28 eV for Ir₂ sits between the values of 1.58 and 2.53 eV from Wang et al. and Dixon et al., respectively.^{11,12} The 5d⁷6s² quartet state of the iridium atom is found to be $\Delta E = 0.58$ eV more favourable than the 5d⁸6s¹ quartet state. The binding energy of the heteronuclear dimer PdIr (1.41 eV) is lower than the average (1.53 eV) of the homonuclear dimers. Any structure can therefore be predicted to maximise homonuclear bonding, as seen in the strongly segregated structures. The lowest spin state of PdIr (quartet) is also an intermediate between those of Ir₂ and Pd₂.

The bulk phase behaviour of the Pd-Ir alloy system shows a significant miscibility gap below 1500°C. Pd-Ir clusters can therefore be predicted to display a strong demixing tendency.²¹ The bulk cohesive energies, shown in table 2, also show the strength of Ir-Ir bonding. The strength of this homonuclear interaction indicates the demixing tendency in the PdIr system.

Cluster of this size are almost all surface. The surface energies of the metals, shown in table 2, can be used to predict that Pd will preferentially occupy low-coordination sites.

Table 1: Binding energies (E_b) and multiplicities ($2S + 1$) of Pd, PdIr and Ir dimers.

Dimer	E_b / eV	($2S + 1$)
Pd ₂	0.78	3
PdIr	1.41	4
Ir ₂	2.28	5

Table 2: Surface and cohesive energies for Pd and Ir.^{22,23}

	Surface Energy / Jm^{-2}	Cohesive Energy / eV/atom
Pd	1.743	3.89
Ir	2.655	6.94

Excess energies can be used to evaluate the effect of mixing in a system. The excess energy (Δ) of a system is defined in equation 1. Δ plots for $N=8-10$ are shown in Figures 6, 7 and 8.

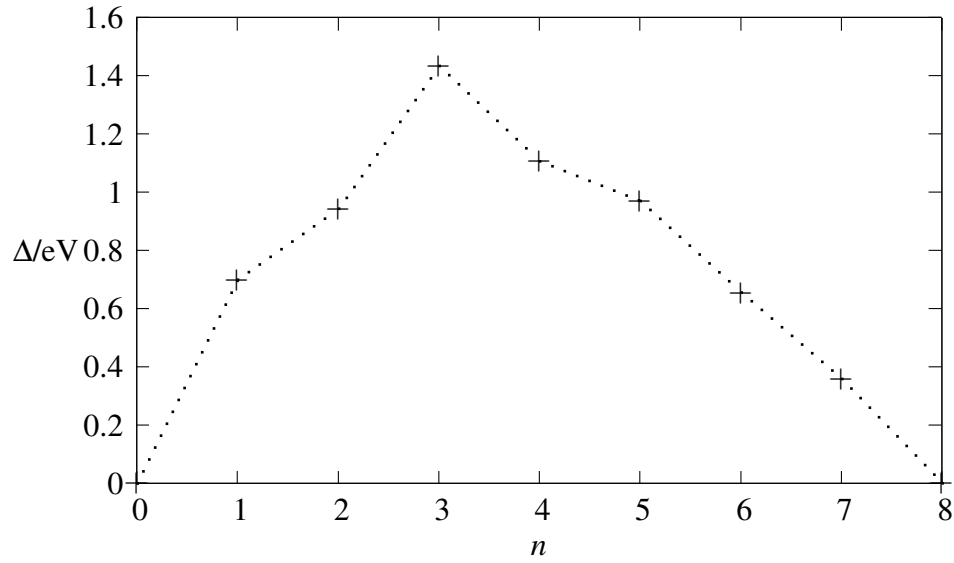


Figure 6: Plot of Δ against the number of Pd atoms for Pd_nIr_{8-n}

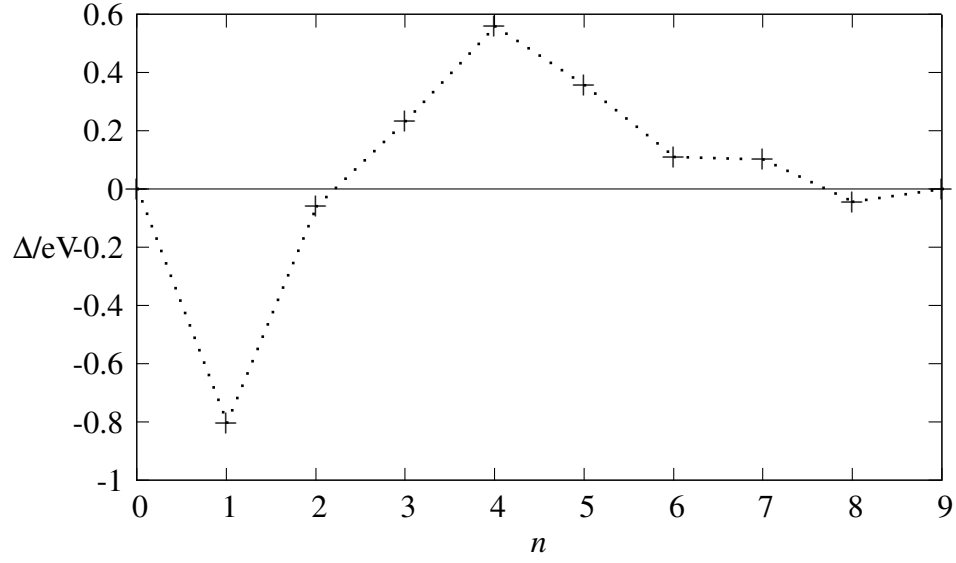


Figure 7: Plot of Δ against the number of Pd atoms for $\text{Pd}_n\text{Ir}_{9-n}$.

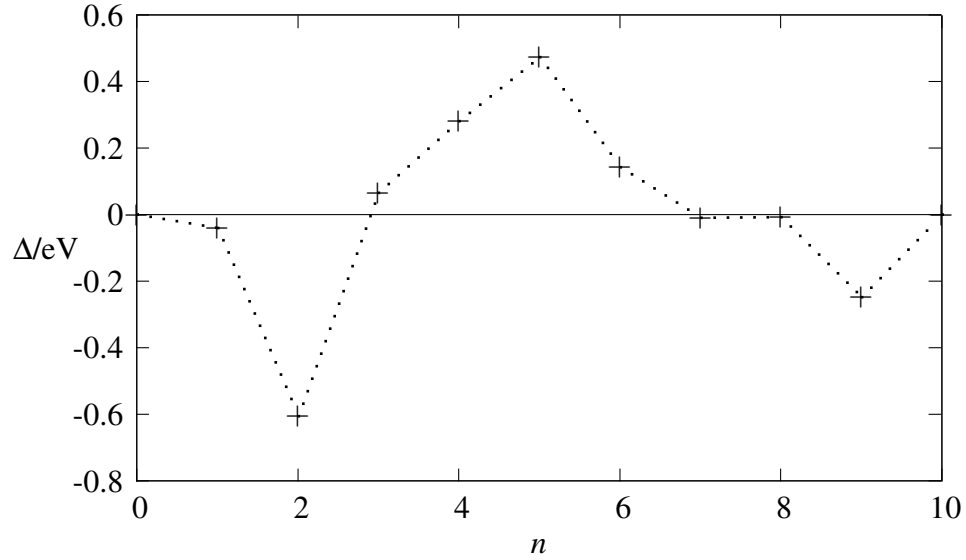


Figure 8: Plot of Δ against the number of Pd atoms for $\text{Pd}_n\text{Ir}_{10-n}$.

The positive Δ values for $\text{Pd}_n\text{Ir}_{(8-n)}$ in Figure 6 demonstrate the strong demixing tendency. The maximum Δ value is seen for Pd_3Ir_5 . For the global minima of $N=9$ and 10 some negative Δ values can be seen, indicating favourable mixing. Negative Δ values are seen for PdIr_8 and Pd_2Ir_8 .

Homotops are inequivalent isomers obtained by swapping the positions of different atom types.

The number of homotops for a system rises combinatorially with size and is maximised for 50/50 compositions. For the 10-atom house-like structures, Pd_2Ir_8 , Pd_3Ir_7 and Pd_4Ir_6 have 45, 120 and 210 homotops, respectively. The number of homotops is reduced if only symmetry inequivalent structures are considered, so the numbers of homotops for Pd_2Ir_8 , Pd_3Ir_7 and Pd_4Ir_6 are reduced to 15, 28 and 59, respectively. To evaluate the ability of the BCGA-DFT to find the GM, all symmetry-inequivalent cubic homotops were reminimised using Quantum Espresso for all three cluster sizes.

The homotop search confirms that the BCGA-DFT search found the lowest energy homotop as the global minima for all but Pd_4Ir_6 . This is shown for Pd_2Ir_6 , Pd_1Ir_8 , Pd_2Ir_7 and Pd_2Ir_8 in figures 9-12. The BCGA was, however, unsuccessful in finding the lowest energy homotop for Pd_4Ir_6 . Figure 13 shows the structural difference between the two lowest energy homotops, 1 and 2, is the placement of the lower Pd-Pd bond. There are three competing factors which determine the homotop stability. Firstly, Pd atoms preferentially tend to occupy low connectivity sites (due to the relative weakness of Pd-M bonds). Secondly, Pd typically occupies capping sites, thereby minimising distortion of the Ir_8 cube. Finally, Pd atoms tend to segregate together, as this maximises the number of (stronger) Ir-Ir bonds.

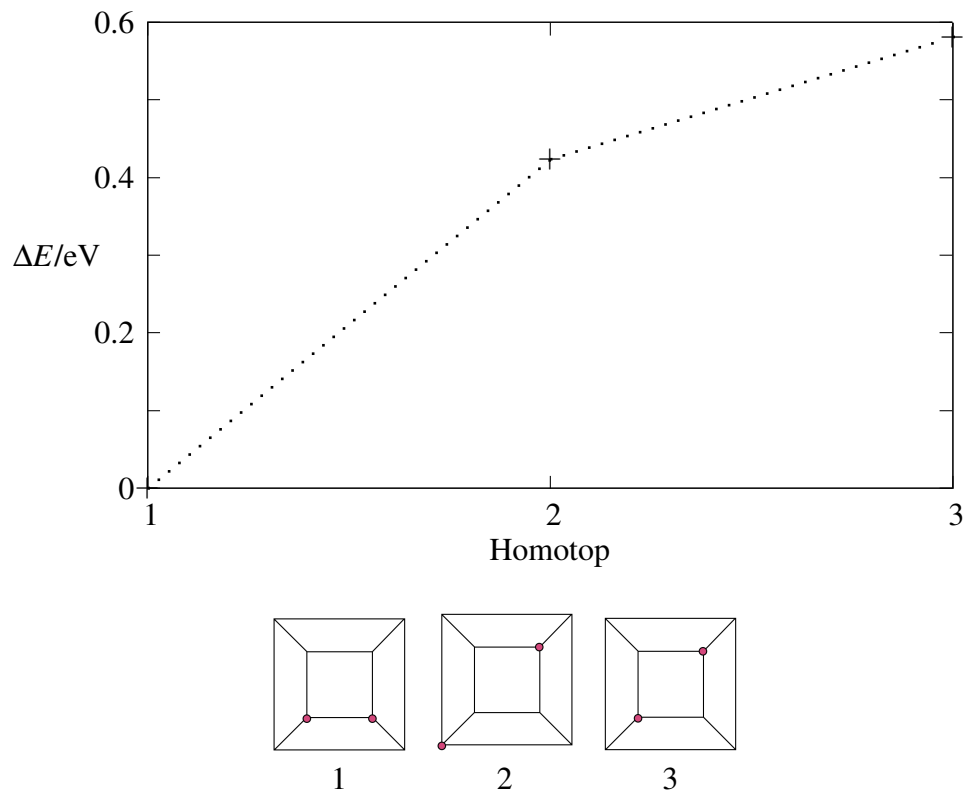


Figure 9: Relative energies of symmetry inequivalent homotop structures for cubic Pd_2Ir_6 , with homotop Schlegel diagrams displayed below in order of increasing energy. Pd is shown by circles.

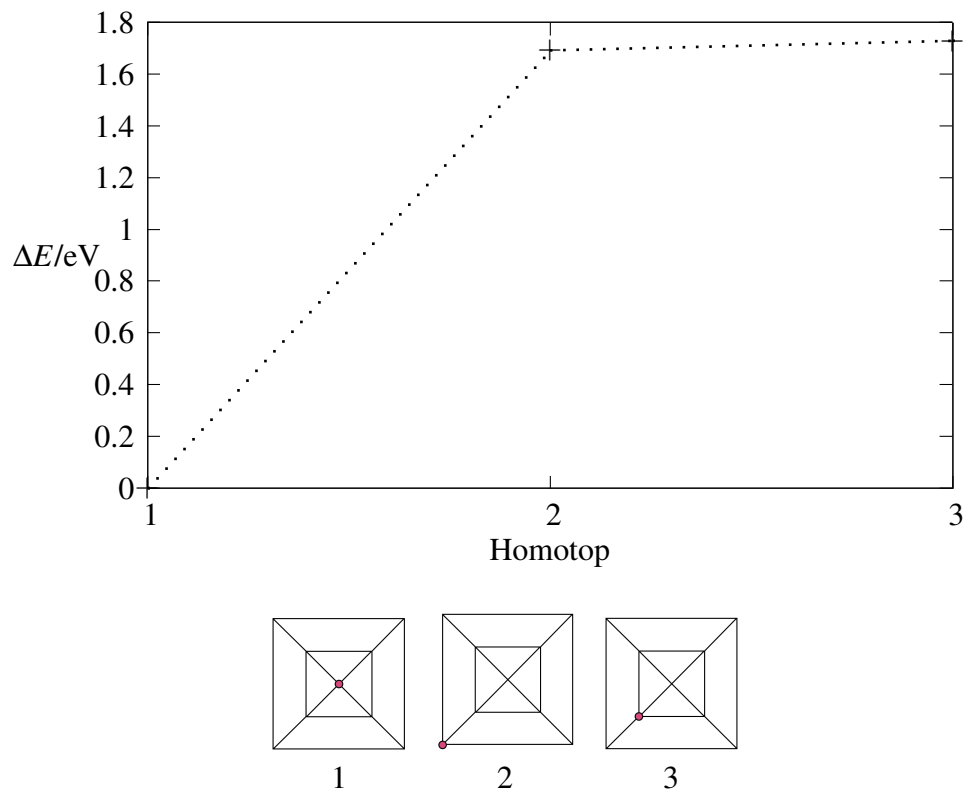


Figure 10: Relative energies of symmetry inequivalent homotop structures for capped cubic Pd_1Ir_8 .

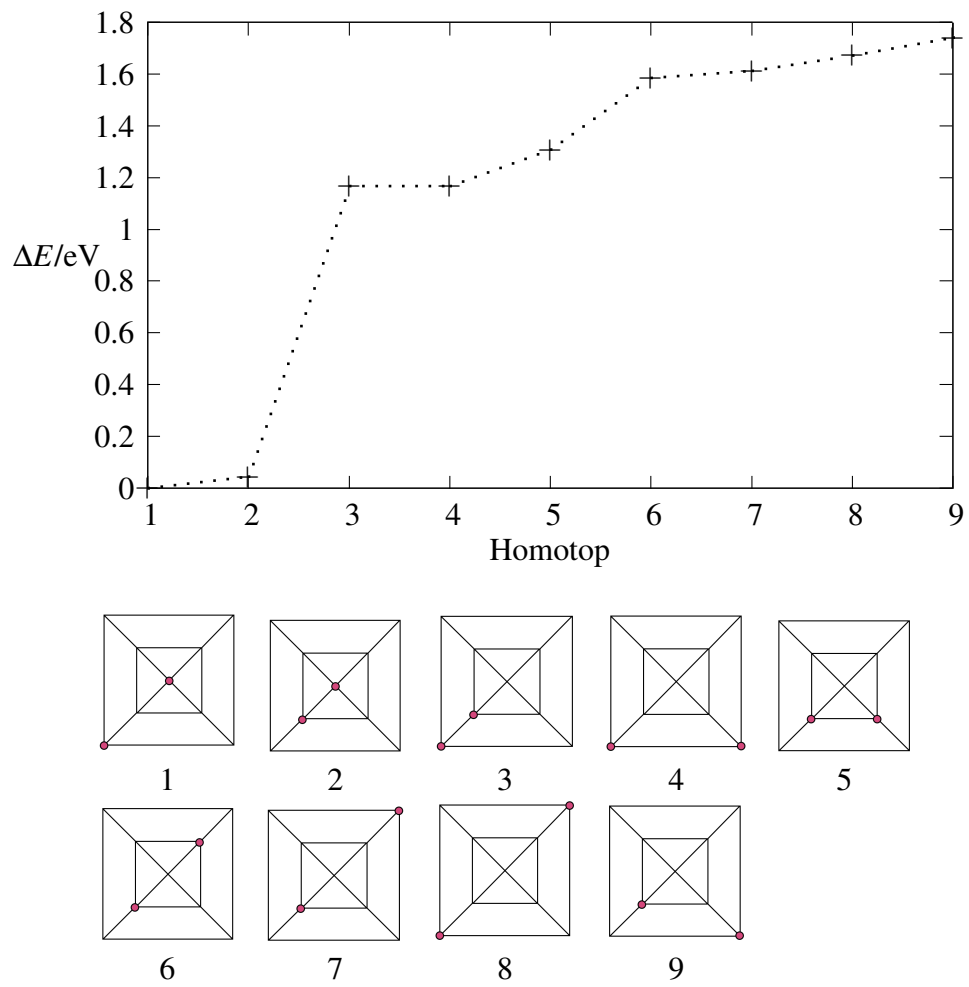


Figure 11: Relative energies of symmetry inequivalent homotop structures for capped cubic Pd_2Ir_7 .

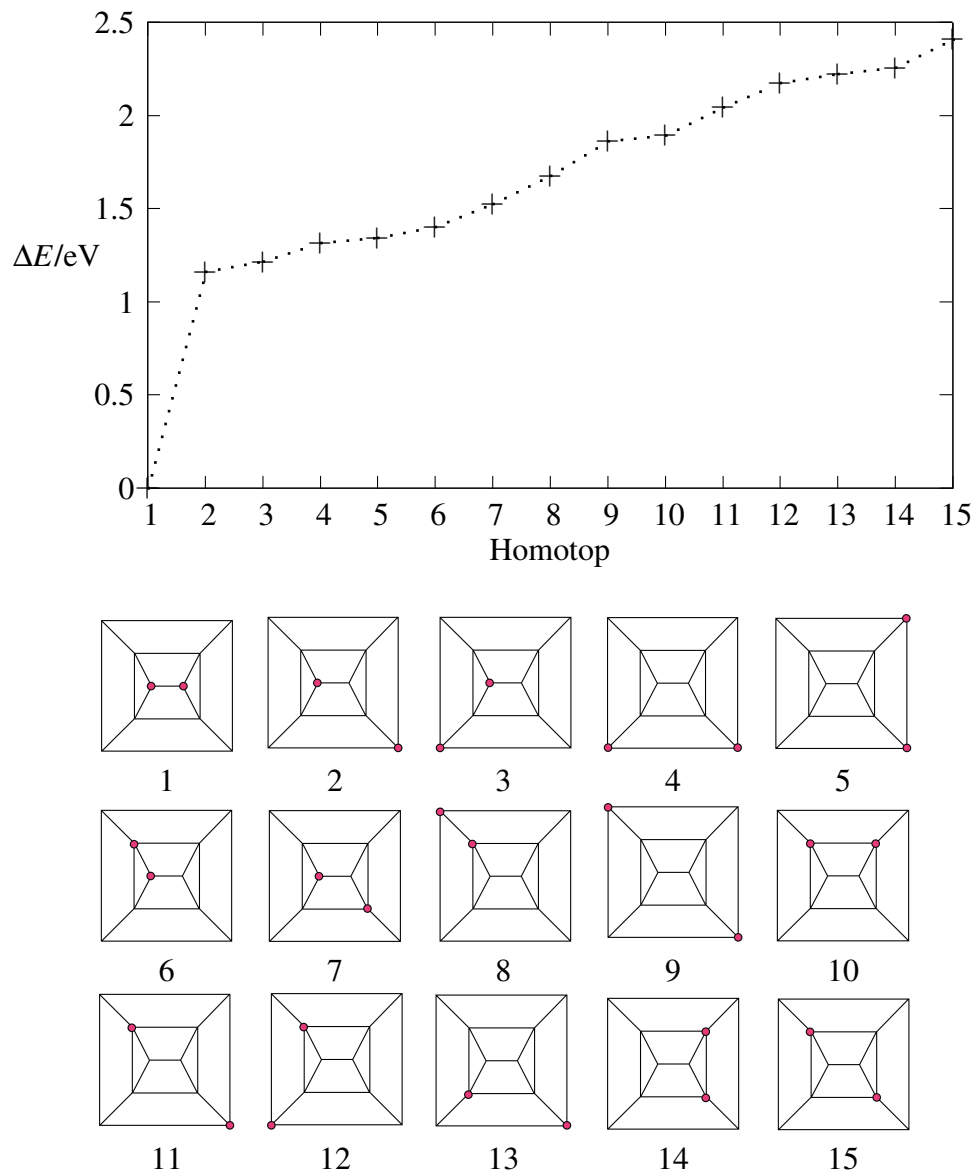


Figure 12: Relative energies of symmetry inequivalent homotop structures for house-like Pd_2Ir_8 .

During the QE geometry optimisation homotop 32 for Pd_4Ir_6 underwent a barrierless transition to the overall GM structure (homotop 2). Figure 14 shows the structural reorganisation through a structure composed of three face-sharing trigonal prisms, taken from the L-BFGS minimisation pathway.

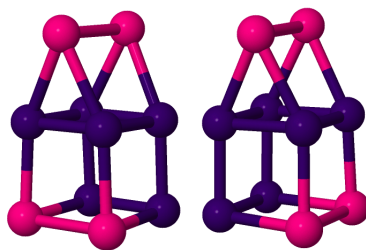


Figure 13: Homotop structures of Pd_4Ir_6 : homotop 1 left, and homotop 2, right

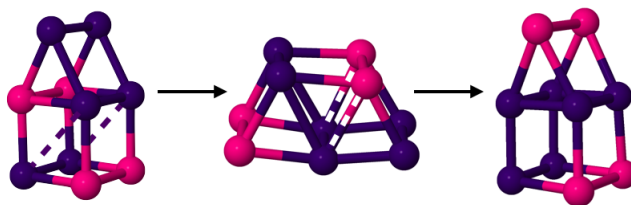


Figure 14: Structural rearrangement of homotop 32 to 2 via the face sharing trigonal prism structure, bond formation and breaking showing by dashed lines and striped line bonds, respectively.

Tables 3-5 display the effect of restricting spin in NWChem reoptimisations of the BCGA-DFT minima for $N=8-10 \text{ Pd}_n\text{Ir}_{(N-n)}$. Each structure was reoptimised for its first 5 lowest multiplicities, the most favourable spin-state being the lowest-energy multiplicity. For those structures whose lowest energy multiplicity was the highest of these values, three-extra spin-states were considered; this was the case for Pd_2Ir_6 , Pd_3Ir_5 and Pd_4Ir_4 . Previous work on Ir_8 has shown it to favour a singlet state.¹⁰⁻¹² Our results suggest Ir_8 has a singlet state, with a low lying ($\Delta E=0.1$ eV) triplet and 13-et state. Ir_9 and Ir_{10} are found to have sextet and triplet states, respectively.

The lowest energy multiplicities of Pd_8 , Pd_9 and Pd_{10} are a quintet, quintet and septet, respectively. Pd_8 is found to favour a higher spin-state than the triplet previously reported.²⁰ There is no clear pattern of lowest energy spin states, as a function of composition for the mixed Pd-Ir clusters.

Table 3: Relative energies ($\Delta E/\text{eV}$) for various multiplicities ($(2S+1)$) of $\text{Pd}_n\text{Ir}_{(8-n)}$ clusters

Ir_8		PdIr_7		Pd_2Ir_6	
$(2S+1)$	ΔE	$(2S+1)$	ΔE	$(2S+1)$	ΔE
1	0	2	0	1	0.563
3	0.102	4	0.179	3	0.137
5	0.108	6	0.162	5	0.127
7	0.225	8	0.108	7	0.141
9	0.245	10	0.122	9	0.08
11	0.252			11	0
13	0.104			13	0.274
15	1.661			15	0.916
Pd_3Ir_5		Pd_4Ir_4		Pd_5Ir_3	
$(2S+1)$	ΔE	$(2S+1)$	ΔE	$(2S+1)$	ΔE
2	0.404	1	0.629	2	0
4	0.429	3	0.272	4	0.173
6	0.284	5	0.189	6	0.32
8	0.075	7	0.125	8	0.408
10	0	9	0.027	10	0.392
12	0.117	11	0		
14	0.392	13	0.122		
16	2.078	15	1.866		
Pd_6Ir_2		Pd_7Ir		Pd_8	
$(2S+1)$	ΔE	$(2S+1)$	ΔE	$(2S+1)$	ΔE
1	0.49	2	0.214	1	0.13
3	0.171	4	0.095	3	0.021
5	0.005	6	0	5	0
7	0	8	0.147	7	0.568
9	0.394	10	0.579	9	1.085

Table 4: Relative energies ($\Delta E/\text{eV}$) for various multiplicities ($(2S+1)$) of $\text{Pd}_n\text{Ir}_{(9-n)}$ clusters

Ir_9		PdIr_8		Pd_2Ir_7	
$(2S+1)$	ΔE	$(2S+1)$	ΔE	$(2S+1)$	ΔE
2	0.028	1	0	2	0
4	0.008	3	0.128	4	0.089
6	0	5	0.192	6	0.15
8	0.124	7	0.354	8	0.157
10	0.214	9	0.488	10	0.173
Pd_3Ir_6		Pd_4Ir_5		Pd_5Ir_4	
$(2S+1)$	ΔE	$(2S+1)$	ΔE	$(2S+1)$	ΔE
1	0.255	2	0.439	1	0.351
3	0	4	0.301	3	0.153
5	0.042	6	0.229	5	0
7	0.175	8	0.113	7	0.022
9	0.049	10	0	9	0.033
		12	0.054		
		14	0.29		
		16	1.707		
Pd_6Ir_3		Pd_7Ir_2		Pd_8Ir	
$(2S+1)$	ΔE	$(2S+1)$	ΔE	$(2S+1)$	ΔE
2	0	1	0.163	2	0.35
4	0.107	3	0	4	0.192
6	0.277	5	0.12	6	0.078
8	0.453	7	0.244	8	0
10	0.66	9	0.244	10	0.497
Pd_9					
$(2S+1)$	ΔE				
1	0.271				
3	0.098				
5	0				
7	0.086				
9	0.788				

Table 5: Relative energies ($\Delta E/\text{eV}$) for various multiplicities ($(2S+1)$) of $\text{Pd}_n\text{Ir}_{(10-n)}$ clusters

Ir_{10}		PdIr_9		Pd_2Ir_8	
$(2S+1)$	ΔE	$(2S+1)$	ΔE	$(2S+1)$	ΔE
1	0.168	2	0.14	1	0
3	0	4	0	3	0.7
5	0.184	6	0.173	5	0.159
7	0.244	8	0.375	7	0.4
9	0.389	10	0.492	9	0.651
Pd_3Ir_7		Pd_4Ir_6		Pd_5Ir_5	
$(2S+1)$	ΔE	$(2S+1)$	ΔE	$(2S+1)$	ΔE
2	0	1	0.254	2	0.095
4	0.005	3	0	4	0.275
6	0.164	5	0.112	6	0
9	0.264	7	0.203	8	0.047
10	0.434	9	0.371	10	0.017
Pd_6Ir_4		Pd_7Ir_3		Pd_8Ir_2	
$(2S+1)$	ΔE	$(2S+1)$	ΔE	$(2S+1)$	ΔE
1	0.273	2	0	1	0.373
3	0.046	4	0.132	3	0.112
5	0	6	0.243	5	0.004
7	0.08	8	0.291	7	0
9	0.098	10	0.44	9	0.067
Pd_9Ir		Pd_{10}			
$(2S+1)$	ΔE	$(2S+1)$	ΔE		
2	0.4	1	0.568		
4	0.0262	3	0.263		
6	0.183	5	0.176		
8	0	7	0		
10	0.356	9	0.433		

The role of spin was further investigated through spin-restricted reoptimisations of 3 extra higher energy minima, for Ir_8 , PdIr_7 and Pd_2Ir_6 . For each composition the GM structure did not change (see supporting information) and no reordering on minima was seen.

Conclusions

The use of the BCGA-DFT method has allowed the global optimisation of $N=8-10$ $\text{Pd}_n\text{Ir}_{N-n}$ nanoalloys. The ability to explore the potential energy surface of the system at the DFT level

has yielded the identification of families of cubic structures for pure Ir and Ir-rich PdIr nanoalloys, which are typically not found using empirical potentials. Results for the monometallic species were found to be largely in agreement with those previously reported.^{11,12,20} The ability of the searches to find the GM was evaluated by assessing the relative energies of symmetry-inequivalent homotops of cubic minima. The BCGA-DFT searches were found to be very reliable, with one exception for Pd₄Ir₆. In this case the systematic homotop search identified a lower energy homotop and a barrier-less transition of homotop 32 to the overall lowest energy structure.

Through the use of spin-restricted reoptimisations on BCGA global minima the role of spin in the system has been considered. Spin has been shown to vary widely depending on composition, showing no real trend in lowest energy multiplicities. The spin of the monometallic species are found to be in good agreement with previous studies.^{12,20} Reoptimisations of low-lying minima has shown no reordering, however, any future studies on this system must include the consideration of spin.

Previous work has on pure Ir clusters has indicated a simple cubic to bulk FCC transition at 48-atoms.¹¹ In future work, the cubic structures of pure Ir and Ir-rich nanoalloys will be explored further. These structural studies will be important in future computational studies of catalysis by Pd-Ir nanoalloys.

Acknowledgement

J. B. A. D. thanks the School of Chemistry, University of Birmingham and EPSRC for his PhD scholarship and Paul C. Jennings for helpful discussions. The authors acknowledge the Engineering and Physical Sciences Research Council, UK (EPSRC) for funding under Critical Mass Grant EP/J010804/1 "TOUCAN: Towards an Understanding of Catalysis on Nanoalloys". Calculations were performed via our membership of the UK's HPC Materials Chemistry Consortium, which is funded by EPSRC (EP/F067496); this work made use of the facilities of HECToR, the UK's national high-performance computing service, which is provided by UoE HPCx Ltd at the University of Edinburgh, Cray Inc. and NAG Ltd, and funded by the Office of Science and Technology

through EPSRC's High End Computing Programme. Calculations were also performed on the EPSRC-funded MidPlus HPC facility, grant EP/K000128/1.

Supporting Information Available

Table 6: Binding energies, structure and point group symmetries for $\text{Pd}_n\text{Ir}_{(8-n)}$ clusters

Composition	E_b eV/atom	Structure	Point Group
Ir_8	-4.65	Cube	O_h
PdIr_7	-4.22	Cube	C_{3v}
Pd_2Ir_6	-3.89	Cube	C_{2v}
Pd_3Ir_5	-3.46	Capped trigonal prism with additional cap on resulting square pyramid	C_s
Pd_4Ir_4	-3.17	Bi-capped trigonal prism	C_s
Pd_5Ir_3	-2.85	Two-atom face-capped octahedron	C_s
Pd_6Ir_2	-2.55	Edge-sharing square pyramid	C_{2v}
Pd_7Ir	-2.26	Capped pentagonal bipyramid	C_s
Pd_8	-1.97	Dodecahedron fragment	D_{2h}

Table 7: Binding energies, structure and point group symmetries for $\text{Pd}_n\text{Ir}_{(9-n)}$ clusters

Composition	E_b eV/atom	Structure	Point Group
Ir_9	-4.64	Edge-capped cube	C_{2v}
PdIr_8	-4.44	Face-capped cube	C_{4v}
Pd_2Ir_7	-4.06	Face-capped cube	C_s
Pd_3Ir_6	-3.74	Face-capped cube	C_s
Pd_4Ir_5	-3.42	Tri-capped trigonal prism	C_s
Pd_5Ir_4	-3.15	Two face-sharing trigonal prisms with cap	C_s
Pd_6Ir_3	-2.89	Two face-sharing octahedra	D_{3h}
Pd_7Ir_2	-2.60	Two face-sharing octahedra	D_{3h}
Pd_8Ir	-2.33	Icosahedral fragment	C_{2v}
Pd_9	-2.03	Icosahedral fragment	C_{2v}

Table 8: Binding energies, structure and point group symmetries for $\text{Pd}_n\text{Ir}_{(10-n)}$ clusters

Composition	Binding Energy eV/atom	Structure	Point Group
Ir_{10}	-4.76	Two-atom face-capped cube	C_{2v}
PdIr_9	-4.50	Two-atom face-capped cube	C_s
Pd_2Ir_8	-4.29	Two-atom face-capped cube	C_{2v}
Pd_3Ir_7	-3.95	Two-atom face-capped cube	C_s
Pd_4Ir_6	-3.66	Two-atom face-capped cube	C_s
Pd_5Ir_5	-3.38	Tri-capped trigonal prism with additional cap on resulting square pyramid	C_s
Pd_6Ir_4	-3.15	Bi-capped face-sharing trigonal pyramid	C_{2v}
Pd_7Ir_3	-2.89	Two face-sharing octahedra with cap	C_{2v}
Pd_8Ir_2	-2.63	Two edge-sharing octahedra	D_{2h}
Pd_9Ir	-2.38	Incomplete fragment of centred Icosahedron	C_{3v}
Pd_{10}	-2.09	Incomplete fragment of centred Icosahedron	C_{3v}

Additional homotop information.

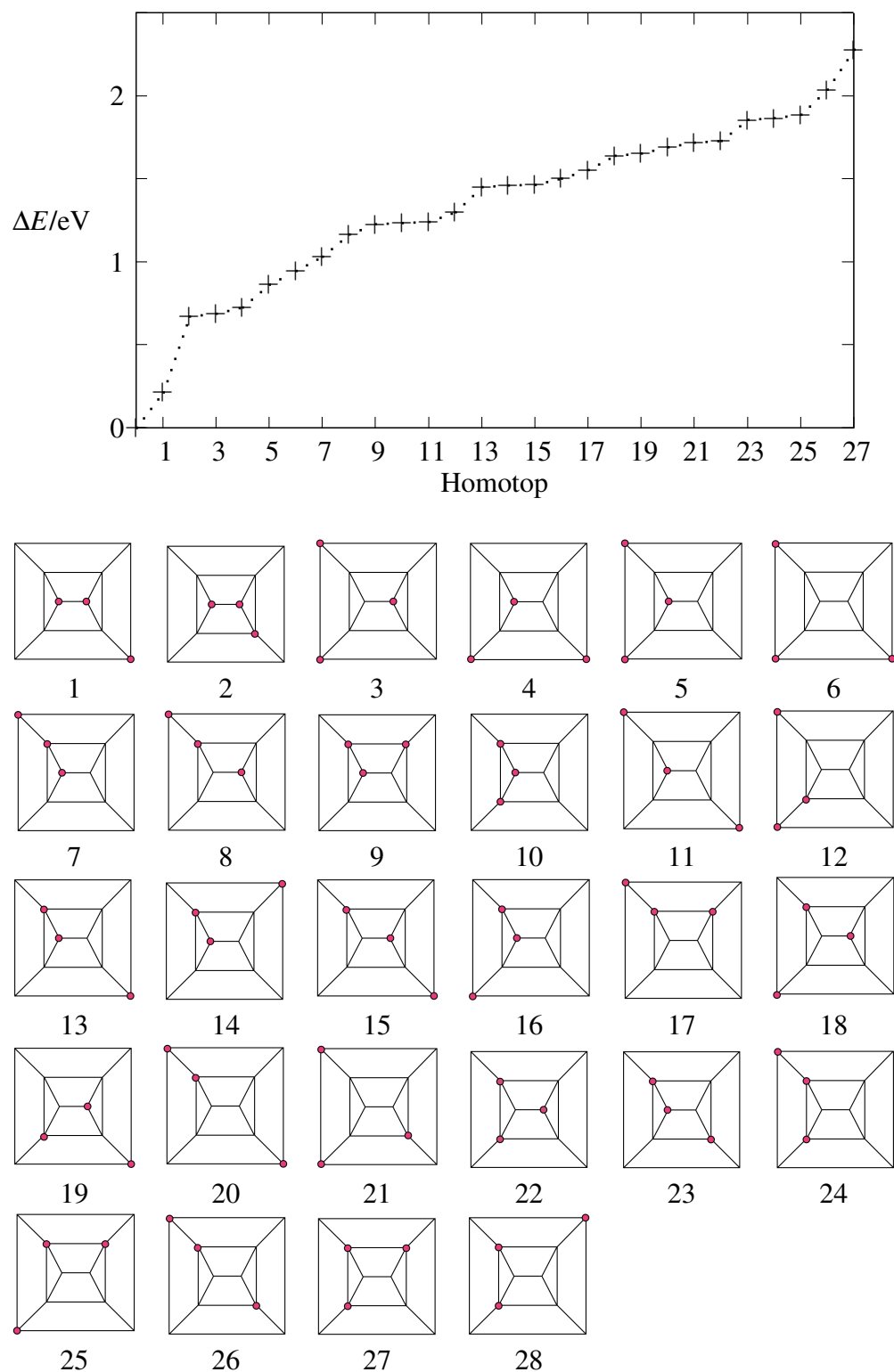


Figure 15: Relative energies of symmetry inequivalent homotop structures for Pd_3Ir_7 , with homotop Schlegel diagrams displayed below graph in the order of increasing energy.

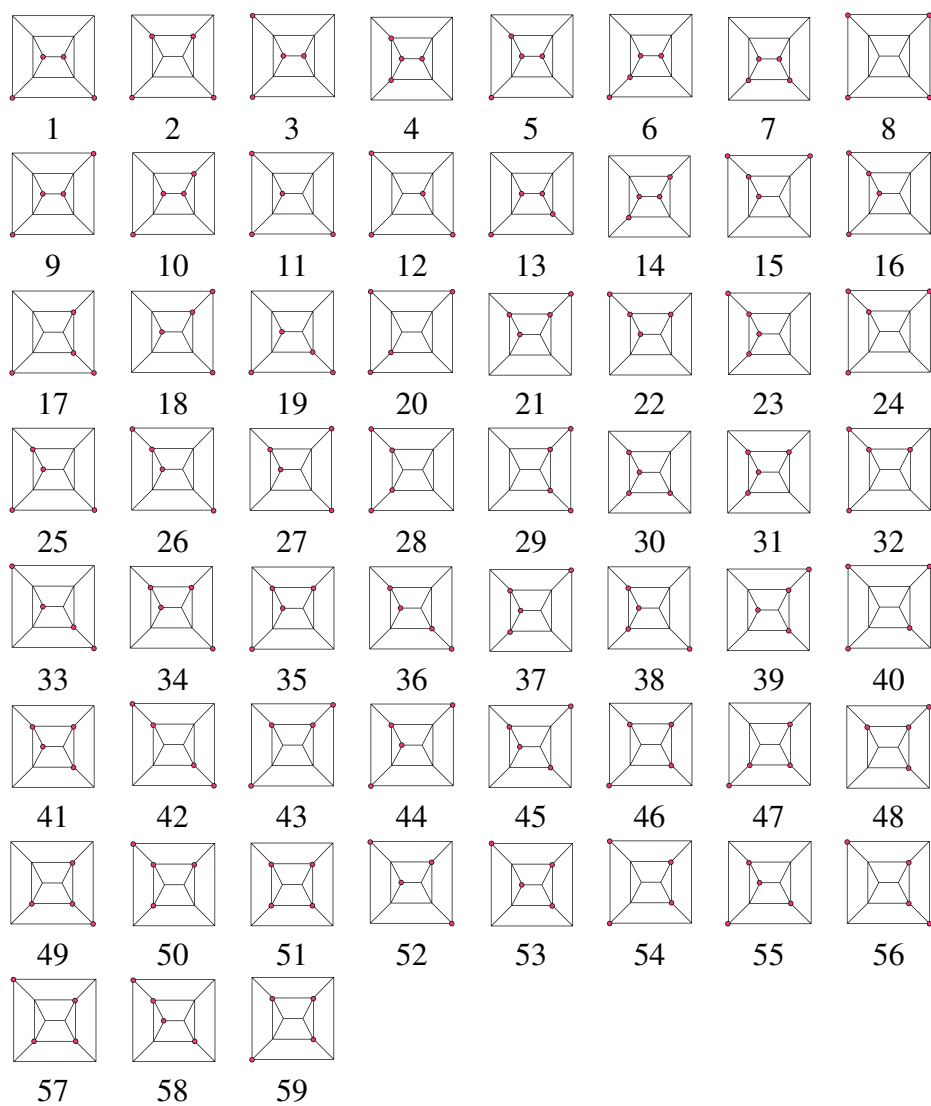
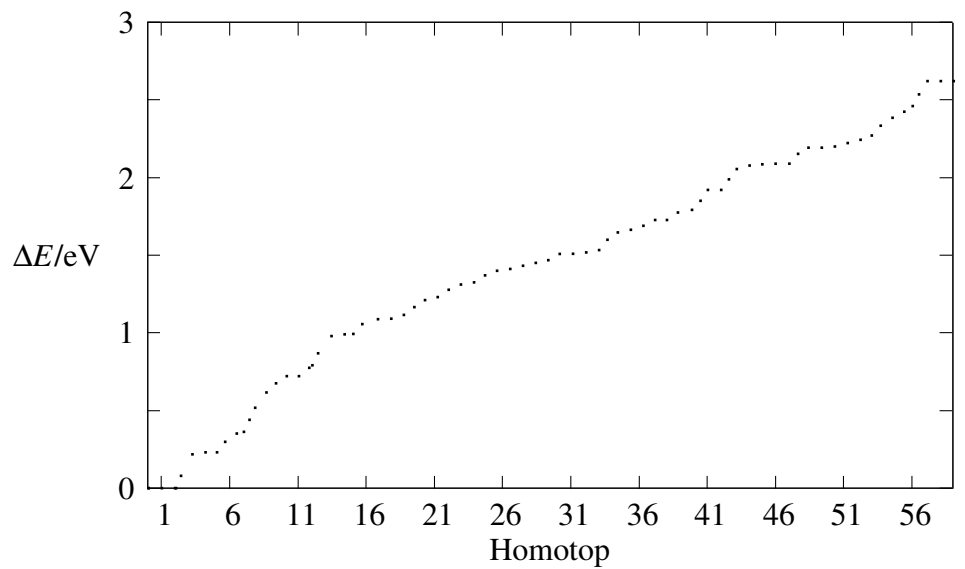


Figure 16: Relative energies of symmetry-equivalent homotop structures for Pd_4Ir_6 .

Table 9: Relative energies ($\Delta E/\text{eV}$) for various multiplicities ($(2S+1)$) of Ir_8 and three higher energy minima from the BCGA-DFT search

1	2	3	4
$(2S+1)$ ΔE	$(2S+1)$ ΔE	$(2S+1)$ ΔE	$(2S+1)$ ΔE
1 0	1 2.76	1 3.31	1 2.74
3 0.1	3 2.33	3 2.67	3 2.25
5 0.11	5 2.29	5 2.66	5 2.45
7 0.22	7 2.12	7 2.52	7 Waiting
9 0.25	9 2.04	9 2.36	9 2.38
11 0.25	11 2.20	11 2.31	11 Waiting
13 0.10	13 2.54	13 2.37	13 Waiting
15 1.66	15 3.09	15 2.71	15 Waiting
17 3.01	17 Waiting	17 3.11	17 Waiting

Table 10: Relative energies ($\Delta E/\text{eV}$) for various multiplicities ($(2S+1)$) of PdIr_7 and three higher energy minima from the BCGA-DFT search

1	2	3	4
$(2S+1)$ ΔE	$(2S+1)$ ΔE	$(2S+1)$ ΔE	$(2S+1)$ ΔE
1 0.56	1 Waiting	1 Waiting	1 1.21
3 0.14	3 0.84	3 0.55	3 0.54
5 0.13	5 0.68	5 0.50	5 0.58
7 0.14	7 0.47	7 0.28	7 0.39
9 0.08	9 0.19	9 0.24	9 0.20
11 0.00	11 0.03	11 0.21	11 0.34
13 0.27	13 0.19	13 0.55	13 0.60
15 0.92	15 0.78	15 1.30	15 1.25
17 2.81	17 2.47	17 2.67	17 Waiting

Table 11: Relative energies ($\Delta E/\text{eV}$) for various multiplicities ($(2S+1)$) of Pd_2Ir_6 and three higher energy minima from the BCGA-DFT search

1	$(2S+1)$	ΔE	2	$(2S+1)$	ΔE	3	$(2S+1)$	ΔE	4	$(2S+1)$	ΔE
	1	0.56		1	Waiting		1	Waiting		1	1.21
	3	0.14		3	0.84		3	0.55		3	0.54
	5	0.13		5	0.68		5	0.50		5	0.58
	7	0.14		7	0.47		7	0.28		7	0.39
	9	0.08		9	0.19		9	0.24		9	0.20
	11	0.00		11	0.03		11	0.21		11	0.34
	13	0.27		13	0.19		13	0.55		13	0.60
	15	0.92		15	0.78		15	1.30		15	1.25
	17	2.81		17	2.47		17	2.67		17	Waiting

This material is available free of charge via the Internet at <http://pubs.acs.org/>.

References

- (1) Sinfelt, J. H. *Bimetallic catalysts: Discoveries, concepts, and applications*; Wiley: New York, 1983.
- (2) Ferrando, R.; Jellinek, J.; Johnston, R. L. *Chemical Reviews* **2008**, *108*, 845–910.
- (3) Jellinek, J.; Krissinel, E. B. *Chemical Physics Letters* **1996**, *4*, 283–292.
- (4) Wales, D. J. *Journal of chemical Physics* **1997**, *101*, 5111–5116.
- (5) Johnston, R. L. *Dalton Transactions* **2003**, 4193.
- (6) Uzun, A.; Dixon, D. A.; Gates, B. C. *ChemCatChem* **2011**, *3*, 95–107.
- (7) Santikunaporn, M.; Herrera, J.; Jongpatiwut, S.; Resasco, D.; Alvarez, W.; Sughrue, E. *Journal of Catalysis* **2004**, *228*, 100–113.
- (8) López-De Jesús, Y. M.; Johnson, C. E.; Monnier, J. R.; Williams, C. T. *Topics in Catalysis* **2010**, *53*, 1132–1137.

- (9) Morfin, F.; Nassreddine, S.; Rousset, J. L.; Piccolo, L. *ACS Catalysis* **2012**, *2*, 2161–2168.
- (10) Zhang, W.; Xiao, L.; Hirata, Y.; Pawluk, T.; Wang, L. *Chemical Physics Letters* **2004**, *383*, 67–71.
- (11) Pawluk, T.; Hirata, Y.; Wang, L. *The journal of physical chemistry. B* **2005**, *109*, 20817–23.
- (12) Chen, M.; Dixon, D. A. *The Journal of Physical Chemistry A* **2013**, *117*, 3676–3688.
- (13) Giannozzi, P.; Baroni, S. *Journal of physics: Condensed matter* **2009**, *21*, 395502.
- (14) Heiles, S.; Logsdail, A. J.; Schäfer, R.; Johnston, R. L. *Nanoscale* **2012**, *4*, 1109–15.
- (15) Heiles, S.; Johnston, R. L. *International Journal of Quantum Chemistry* **2013**, (in press).
- (16) Sansonetti, J. E.; Martin, W. C. *Journal of Physical Chemistry Reference Data* **2005**, *34*, 1777–1781.
- (17) Valiev, M.; Bylaska, E.; Govind, N.; Kowalski, K.; Straatsma, T.; Van Dam, H.; Wang, D.; Nieplocha, J.; Apra, E.; Windus, T.; de Jong, W. *Computer Physics Communications* **2010**, *181*, 1477–1489.
- (18) Deaven, D.; Ho, K. *Physical Review Letters* **1995**, *75*, 288–291.
- (19) Weigend, F.; Ahlrichs, R. *Physical chemistry chemical physics* **2005**, *7*, 3297–305.
- (20) Nava, P.; Sierka, M.; Ahlrichs, R. *Physical Chemistry Chemical Physics* **2003**, *5*, 3372.
- (21) Tripathi, S. N.; Bharadwaj, S. R.; Chandrasekharaiah, M. S. *Journal of Phase Equilibria* **1991**, *12*, 603–605.
- (22) Tyson, W.; Miller, W. *Surface Science* **1977**, *62*, 267–276.
- (23) Kittel, C. *Introduction to Solid State Physics*, 6th ed.; John Wiley & Sons, 1986; p 55.

Graphical TOC Entry

